Carbohydrate Polymers 99 (2014) 91–97

Contents lists available at ScienceDirect

Carbohydrate Polymers

journal homepage: www.elsevier.com/locate/carbpol

Development of regenerated cellulose/halloysites nanocomposites via ionic liquids

Nurbaiti Abdul Hanid [a], Mat Uzir Wahit [b,*], Qipeng Guo [c], Shaya Mahmoodian [a], Mohammad Soheilmoghaddam [a]

[a] Department of Polymer Engineering, Faculty of Chemical Engineering, 81310 Universiti Teknologi Malaysia, Johor, Malaysia
[b] Center for Composites, 81310 Universiti Teknologi Malaysia, Johor, Malaysia
[c] Polymers Research Group, Institute for Frontier Materials, Deakin University, Geelong, Victoria 3216, Australia

ARTICLE INFO

Article history:
Received 6 April 2013
Received in revised form 3 July 2013
Accepted 26 July 2013
Available online 14 August 2013

Keywords:
Regenerated cellulose
Ionic liquid
EMIMCl
Halloysites
Nanocomposites

ABSTRACT

In this study, regenerated cellulose/halloysites (RC/HNT) nanocomposites with different nanofillers loading were fabricated by dissolving the cellulose in 1-ethyl-3-methylimidazolium chloride (EMIMCl) ionic liquid. The films were prepared via solution casting method and were characterized by X-ray diffraction (XRD), scanning electron microscopy (SEM) and transmission electron microscopy (TEM). The mechanical properties were investigated by tensile testing. It clearly displayed a good enhancement of both tensile strength and Young's modulus with HNT loading up to 5 wt%. As the HNT loadings increased to 5 wt%, the thermal behaviour and water resistance rate was also increased. The TEM and SEM images also depicted even dispersion of the HNT and a good intertubular interaction between the HNT and the cellulose matrix.

1. Introduction

Recently, the development of natural biopolymer materials has received enormous interest as a substitute for non-biodegradable petroleum based plastics. Biopolymer materials are polymers that are biodegradable. The input materials for the production of these polymers may be either renewable or synthetic. There are four main types of biopolymer including starch, sugar, cellulose and synthetic materials. Current and future developments in biodegradable polymers and renewable materials focus mainly on the improvement of product properties but not as an alternative solution to the insecurity of petroleum supplies or to reduce the environmental threat (Wu, Wanga, Li, Li, & Wanga, 2009). Besides being available on a sustainable basis, biopolymer materials have several economic and environmental advantages due to their low cost, availability from renewable sources and their ability to replace some synthetic polymers (Tang, Kumar, Alari, & Sandeep, 2012).

Cellulose was used in this study because it is the most abundant natural polymer on earth and can easily be obtained from wood pulp and cotton. Cellulose has excellent mechanical properties and thermal performance (Nishino, Matsuda, & Hirao, 2004). Cellulose is an important renewable resource and is regaining importance as renewable chemical resources to replace petroleum-based materials (Ma, Zhou, Li, Li, & Ou, 2011; Delhom, White-Ghoorahoo, & Pang, 2010). Therefore, effective utilization of cellulose not only reduces the consumption of our limited fossil resources but also protects the environment. Nowadays, 'green' composites have grabbed a lot of attention because of their unique properties such as outstanding transparency, mechanical properties, non-toxicity and also high biodegradability rate (Takagi & Asano, 2008). However, there were difficulties in processing and regenerating the cellulose as cellulose has a hydrogen bond and a partially crystalline structure which are the main obstructions for dissolving or regenerating cellulose in conventional solvent (Cao et al., 2009).

Recently, ionic liquids (ILs), a new class of 'green' solvent have drawn much attention due to their distinctive properties such as non-volatility, non-flammability, chemical and thermal stability and ease of recycling (Heinze, Schwikal, & Barthel, 2005; Feng & Chen, 2008). Although there are a wide range of ILs, 1-ethyl-3-methylinidazolium chloride (EMIMCl), a molten salt which exists as a liquid at relatively low temperature (<100 °C), was employed to produce the regenerated cellulose. The EMIMCl showed a trend for higher dissolution of cellulose (Vitz, Edmenger, Haensch, & Schubert, 2009).

Halloysites (HNT) occur in great deposits and are a weathering product found in diverse rock structures ranging from volcanic rocks to granite. It is mainly composed of aluminosilicate with the

* Corresponding author. Center for Composites, Universiti Teknologi Malaysia (UTM), 81310 Skudai, Johor, Malaysia. Tel.: +6 07 553 5909; fax: +6 07 553 6165.
E-mail address: mat.uzir@cheme.utm.my (M.U. Wahit).

0144-8617/$ – see front matter © 2013 Elsevier Ltd. All rights reserved.
http://dx.doi.org/10.1016/j.carbpol.2013.07.080

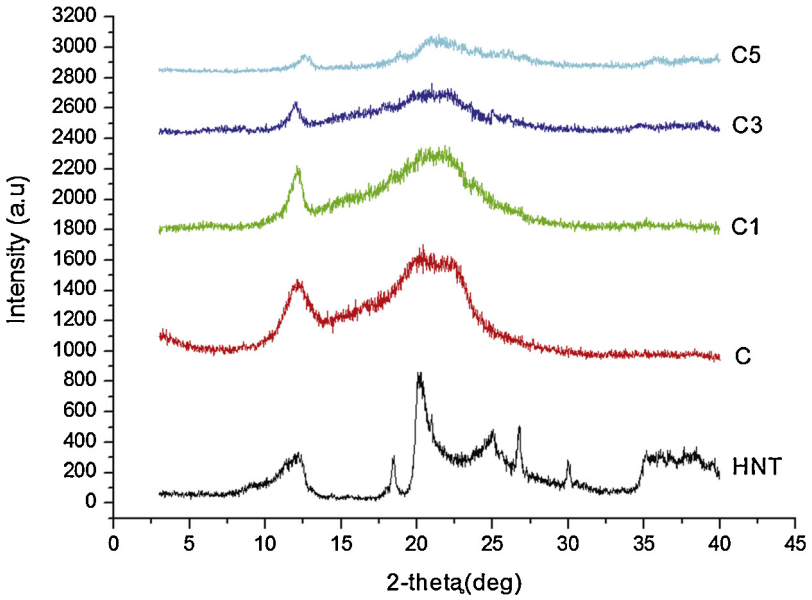

Fig. 1. XRD patterns of C, C1, C3, C5 and HNT.

molecular formula $Al_2(OH)_4Si_2O_5(2H_2O)$. Common halloysites can be found in the form of fine, tubular structures with a length of 300–1500 nm, and with inner and outer diameters of 15–100 nm and 40–120 nm, respectively (Du, Guo, Lei, & Jia, 2007). Du et al. (2007) reported that the HNT nanotubes are more easily dispersed in polymer matrix by shearing due to their rod-like geometry and limited intertubular contact area. HNT are rigid materials and the unique crystal structure of HNTs resembles that of carbon nanotubes (CNTs) in terms of aspect ratio. HNT nanotubes are readily obtainable, are much cheaper than other nanofillers such as carbon nanotubes and are biocompatible (Vergaro et al., 2010).

A recent comprehensive study highlights the benefits and results obtained by reinforcing the halloysite in polyamide 6 (Hedicke-Hochstotter, Lim, & Altstadt, 2009). Moreover, there were reports available in the literature which examined the mechanical and structural properties of melt processed HNT filled polypropylene (PP) nanocomposites as well as investigations into the properties of nanocomposites prepared via dilution of HNT filled PP master batches (Du et al., 2007; Liu, Guo, Du, Chen, & Jia, 2009; Ning et al., 2007; Prashantha, Lacrampe, & Krawczak, 2010). To the best of our knowledge, there are no reports available on a detailed investigation into the preparation of cellulose/halloysites nanocomposites via ionic liquids, EMIMCl.

Our previous work is related to the preparation of regenerated cellulose/montmorillonite nanocomposites films using different types of ionic liquid (1-butyl-3-methylimidazolium chloride (BMIMCl) (Mahmoudian, Wahit, Ismail, & Yussuf, 2012). The results exhibited that the thermal and mechanical properties of the fabricated films were improved. Therefore, the present work aims to develop regenerated cellulose nanocomposites by using the EMIMCl as a solvent with the incorporation of halloysites nanofillers. The effects of halloysite content were characterized.

2. Experimental

2.1. Materials

Microcrystalline cellulose (MCC) with an average size of 50 μm (Avicel), 1-ethyl-3-methylimidazolium chloride (EMIMCl) with ≥95% purity and halloysites nanotubes (HNT) was purchased from Sigma–Aldrich.

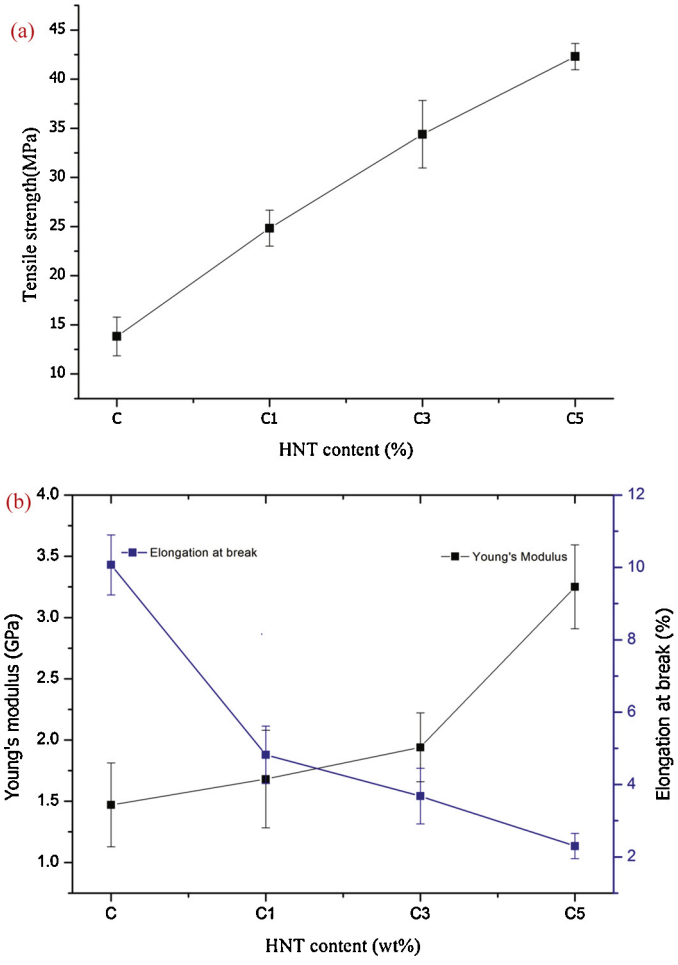

Fig. 2. (a) Tensile strength and (b) elongation at break and Young's modulus values of cellulose nanocomposites with various HNT content.

2.2. Preparation of the nanocomposite film

The cellulose was dried for 3 h at 70 °C. It was then dissolved in the ionic liquid (EMIMCl) at 85 °C for 4 h using a magnetic

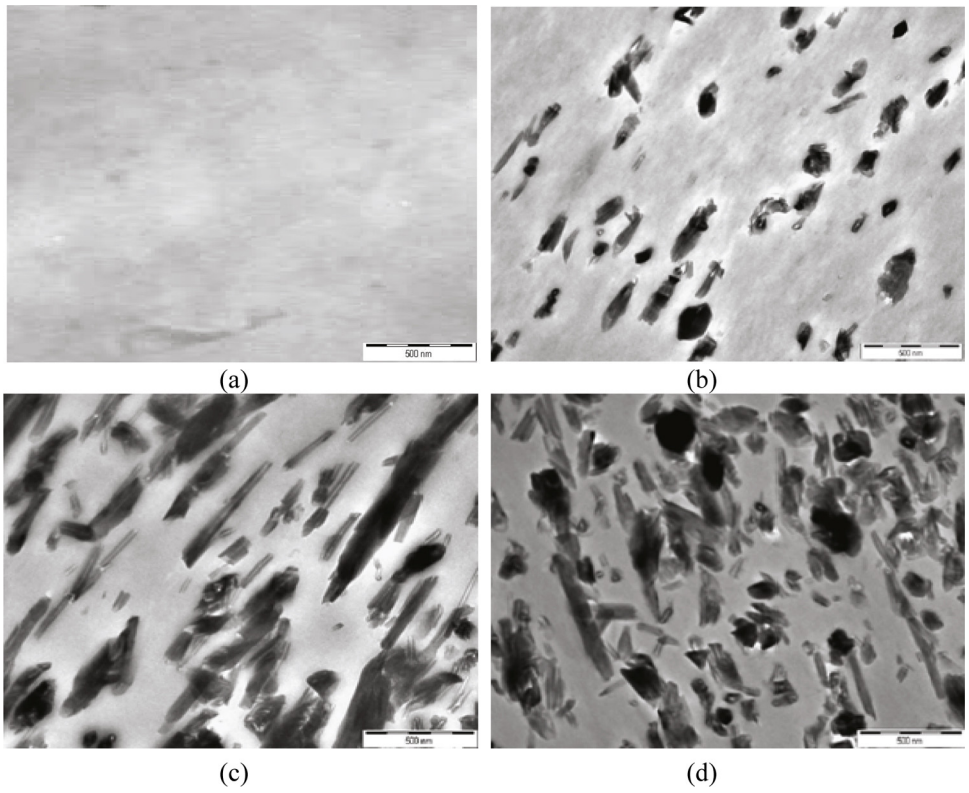

Fig. 3. Transmission electron micrographs of halloysite nanocomposites (a) C1, (b) C1, (c) C3 and (d) C5 (magnification: 25K×).

stirrer. The ratio of cellulose:EMIMCl was 6:94 (wt/wt%). At the same time, the HNT was dispersed in EMIMCl with magnetic stirring for 1 h. Both mixtures were stirred together for 24 h at 85 °C. The air bubble was taken off in the vacuum oven. The solution was cast on a glass plate until a thickness of 0.5 mm was reached and immersed in a water bath for 24 h to remove the entire solvent residue. The film was dried in a vacuum oven at 50 °C for 2 h. Then, formulations of different HNT content (1 wt% (C1), 3 wt% (C3) and 5 wt% (C5) with respect to cellulose content) were prepared with the same procedures as above. The nanocomposites film without HNT loading was identified as C.

3. Characterization

The film was examined by X-ray diffractometer (XRD). The XRD test was performed using a Rigaku Miniflex II desktop X-ray diffractometer. The data was recorded at a scanning speed of 0.02°/min from $2\theta = 2°–40°$. Tensile properties were measured using LRX Tensile Testing Machine which complies with ASTM D882-10. The samples were cut into strips with dimensions of 60 mm × 13 mm × 0.5 mm. The crosshead speed rate was fixed at 10 mm/min. Fractured tensile surfaces were observed using Philip XL SEM at an acceleration voltage of 20 kV. The samples were characterized due to the films morphology such as the shape of the surface material, the texture of the matrix layers and the dispersion of the nanofiller in between the matrix layers. The TEM samples underwent the microtome process using a Power Tome XL. The sample was embedded in resin and left to dry before it was cut with a diamond knife at a thickness of about 100 nm. The film was positioned on a cooper grid before viewed via TEM (Philips CM12).

4. Results and discussions

4.1. X-ray diffractometer (XRD)

The XRD patterns in Fig. 1 demonstrated the X-ray diffractograms of the nanocomposites films. The basal spacing reflections of the HNT indicates a sharp peak at $2\theta = 12.20°$, which translate to basal spacing of 7.35 Å. The presence of basal reflection at $2\theta = 24.50°$ is evidence of dehydration. The XRD profiles of regenerated cellulose (RC) are shown in Fig. 1. The pure RC was identified as C and the RC nanocomposites were identified as C1, C3 and C5, with 1 wt %, 3 wt % and 5 wt % HNT loading, respectively. It is found that upon dissolution and regeneration of cellulose in EMIMCl, the appearance of RC characteristic diffraction angle were displayed at $2\theta = 12°$ corresponds to $(1\bar{1}0)$ plane, while peak at $2\theta = 20.0°$ and $2\theta = 22.0°$ corresponded to (110) and (020) planes, respectively. These peaks are also known as the crystalline structure of cellulose II (Rahatekar et al., 2009). The transformation of crystalline structure from cellulose I to cellulose II exhibited significant similarity to the diffraction angles of RC (Suresh, Yun, & Kim, 2011; Zhao et al., 2012). Peaks located at lower angle, $2\theta = 12°$ and $2\theta = 22.0°$, indicated the presence of structures with limited intercalation and can be attributed to the formation of nanocomposites (Ismail, Pasbakhsh, Ahmad Fauzi, & Abu Bakar, 2008). The appearance of diffraction peaks for HNT are expected at $2\theta = 20.2°$ and $2\theta = 25.0°$. The sharp peak at $2\theta = 20.2°$ for HNT still can be observed due to the fact that the peak was overlapped with the peak for RC since both of the peak appeared at the same diffraction angle. Even though without the incorporation of HNT nanotubes, peak $2\theta = 20.2°$ can clearly be observed in C, which is the pure RC. Nevertheless, it can be observed clearly that the peak at $2\theta = 25.0°$ was totally disappeared with the addition of HNT in the polymer

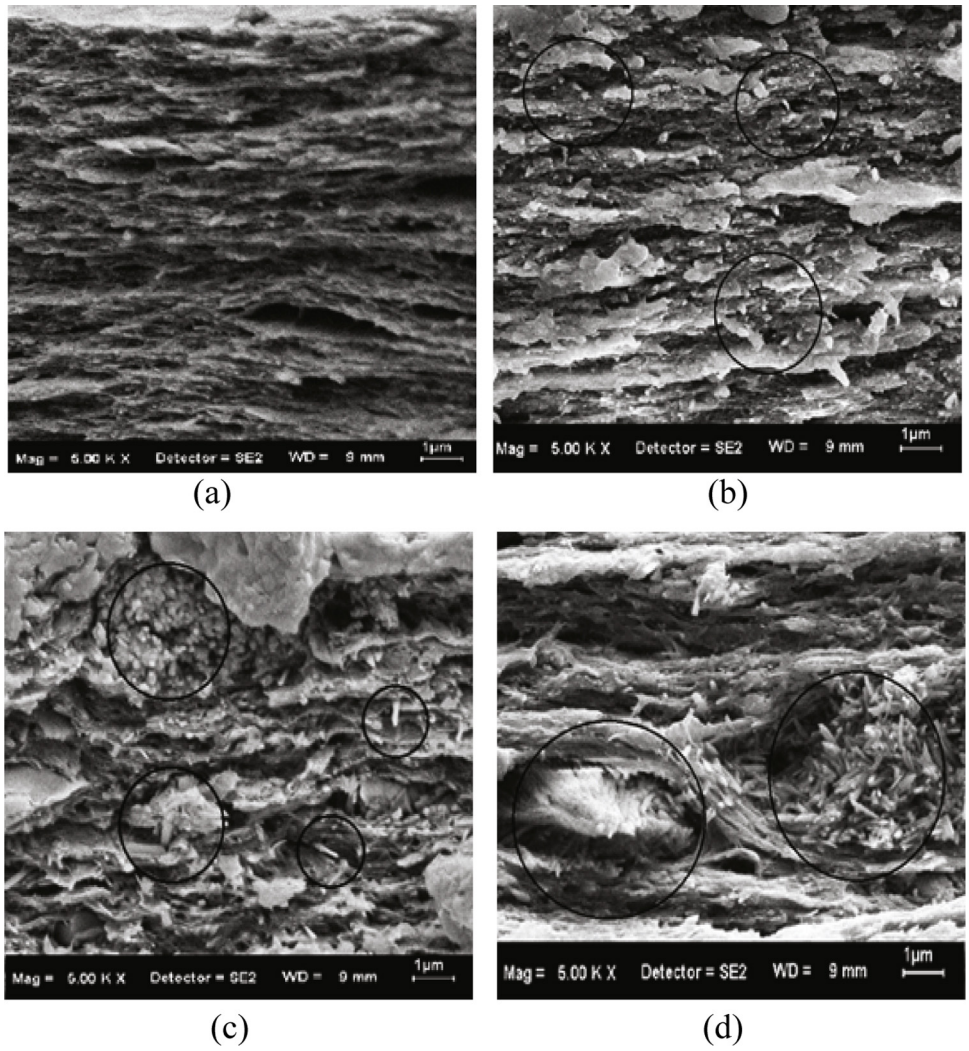

Fig. 4. TEM image of HNT intertubular lumen (magnification: 140K×).

matrix as illustrated for C1, C3 and C5 in Fig. 1, indicating that all the HNT nanotubes were almost fully intercalated. The dispersion and intercalation of the HNT nanotubes can be observed in the TEM images as discussed in following sections. Tang et al. (2011) also reported similar phenomenon in an investigation of the effects of unfolded and intercalated halloysites on the mechanical properties of halloysite–epoxy nanocomposites.

4.2. Mechanical properties and morphology

Fig. 2 shows the tensile strength RC/HNT nanocomposites. The graph revealed that the tensile strength of the fabricated cellulose/HNT nanocomposites was proportional with the increment of the filler loading. C1, with 1 wt% HNT content, exhibited a 44.4% increase in tensile strength compared to C. Similar results were seen in C3 and C5, which had 59.8% and 67.3% higher tensile strength compared to C film, respectively. This is due to the fact that additional filler loading attributed to the agglomeration of the HNT cylindrical nanotubes. The increment of the filler loading enhanced the filler attraction force within the HNT tubes, thus decreasing the surface area for the stress transfer (Handge, Hedicke-Hochstotter, & Altstadt, 2010; Vadukumpully, Paul, Mahanta, & Valiyaveettil, 2011). Therefore, the film with high filler loadings has higher tensile strength compared to the pristine regenerated film. The increasing strength of the nanocomposites films with increments of HNT content was also revealed by the TEM images as discussed in following sections. It is evident that increments of the fillers content could also be ascribed to the formation of agglomerates. The presence of high HNT content causes stress concentration at the fillers surface.

Fig. 2(b) illustrated the Young's modulus and elongation at break for the RC and RC/HNT nanocomposites at various filler contents. It was shown that with the incorporation of HNT, the Young's modulus of the films increases with the addition of the HNT loadings. For C1 and C3, the Young's modulus increased significantly (12.5% and 24.7%, respectively) compared to C. C5 exhibited a remarkable 54.8% increment of Young's modulus compared to C. This is due to the existence of the interaction of the HNT tubes which formed a zig-zag structure (Ismail et al., 2008) that prevented the molecular orientation of the polymer chain, thus enhancing the modulus. Prashantha et al. (2010) also reported significant enhancement with the addition of the HNT loadings. Nevertheless, the elongation at break values decreased with increases in HNT loadings. The elongation at break for C dropped from 10.07% to 4.84% with 1 wt% HNT loading. The elongation at break values reduced continuously with the increment of the HNT loadings as depicted in Fig. 2(b).

The above result was supported with the SEM images as discussed in following sections, which illustrated that at high content of HNT loading, agglomeration occurred which can undergo matrix-filler interaction. The agglomeration of the HNT in the polymer

matrix restricted the movement of the matrix chain. This is due to the fact that the film becomes more rigid at high filler loading, therefore resulting in decreased elongation at break values. Hedicke-Hochstotter et al. (2009) also observed that the reduction of the elongation at break values on halloysite/polyamide nanocomposites was due to a stronger agglomeration of the fillers at high halloysite content. Meanwhile, Lopez Machando, Valentini, Biagiotti, and Kenny (2005) also encountered the same effect on single-wall carbon nanotubes (SWCNT) composites, which also agglomerates at higher SWCNT loading.

4.3. Transmission electron microscopy (TEM)

Fig. 3 showed the TEM images of the HNT nanocomposites. The dispersion of HNT nanotubes were observed in Fig. 3(a, b, c and d) which consist 0 wt%, 1 wt %, 3 wt% and 5 wt% HNT loadings, respectively. The dark dots were the HNT tubes. The HNT can be easily dispersed in the polymer matrix due to its special characteristics which include a silica layer located on the outer surface layer, while alumina was positioned on the inner walls and at the edges of the tube (Levis & Deasy, 2002; Ye, Chen, Wu, & Ye, 2007).

Fig. 3(a) depicted the TEM image of pure RC film without the incorporation of HNT, which showed the sample was clear from the HNT nanotubes. Fig. 3(b, c and d) shows the interaction between the HNTs. Fig. 3(b) depicted the interaction of C1 at low HNT loading (1 wt%). The HNT tubes tend to align by themselves compared to the C3 with higher HNT loading (3 wt%) in Fig. 3(c) where it can clearly be seen that the zig-zag structures were formed between the HNTs. Some of them were formed by edge to edge interactions between the HNTs, while others were formed face to edge. As the HNT loading increased up to 5 wt% as illustrated in Fig. 3(d) of C5, they not only increased the formation of the zig-zag structures, but also have the tendency to agglomerate. This explained the reduction of the elongation at break values which reduced with the increment of the filler loadings. The lumen structure of HNT as shown in Fig. 4 can be filled with the matrix. The penetration of the cellulose matrix material inside the tubes formed the intertubular interaction, thus enhancing the films performance. This phenomenon was also reported by Ismail et al. (2008) which found good penetration of EDPM inside the HNT lumen.

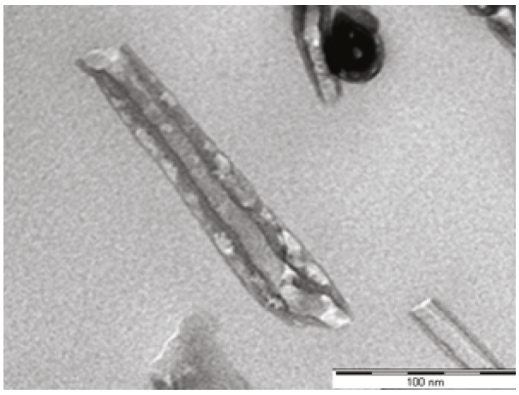

Fig. 5. Tensile fracture surfaces of cellulose/HNT nanocomposites with (a) C, (b) C1, (c) C3 and (d) C5.

4.4. Scanning electron microscopy (SEM)

The scanning electron micrographs revealed that single HNT nanotubes can be uniformly dispersed in cellulose. Fig. 5(a) showed the RC nanocomposites (C) without the addition of HNT. The layers of cellulose matrix can be seen clearly. Fig. 5(b), (c) and (d) shows the dispersion of the HNT in the cellulose matrix for C1, C3 and C5, respectively. Fig. 5(b) showed the C1 films with several broken HNTs (shown by the circle) on the fractured surface of a tensile specimen with obvious separations of the HNT from the matrix, while Fig. 5(c) provides some examples of pull-out of HNTs from the matrix hollows and left in the polymer matrix of C3. Fig. 5(d) also depicted some HNT agglomerates on the fracture surfaces of the C5 nanocomposites film. These agglomerates were not broken up during the dispersion process and decreased the mechanical performance because of stress concentration at large agglomerates (Deng, Zhang, & Ye, 2009). Therefore, it is also understandable that the elongation at break was reduced if the nanotubes were not evenly distributed in the matrix with the presence of large aggregations that cause failure.

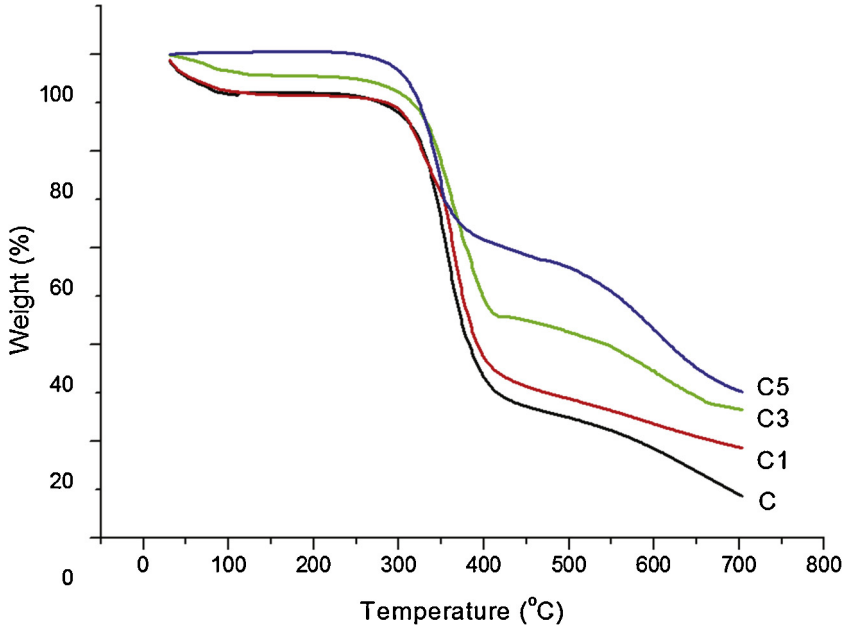

Fig. 6. TGA curves of cellulose/HNT nanocomposites.

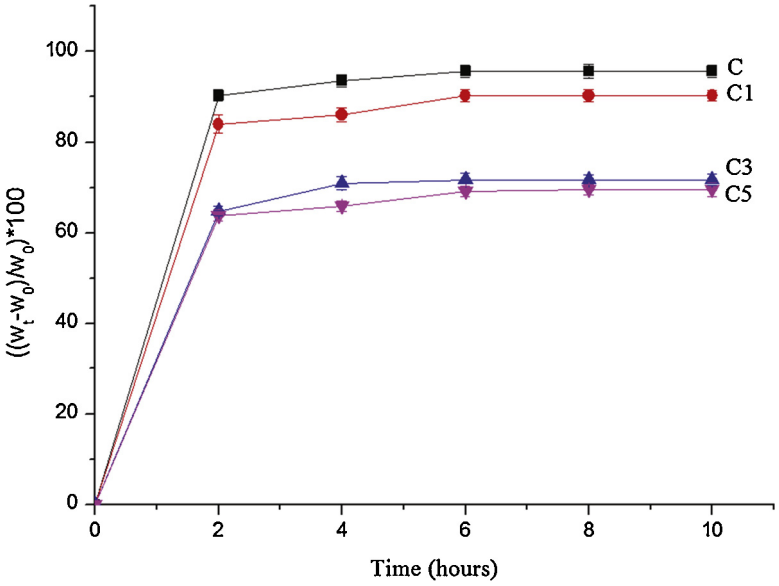

Fig. 7. Moisture absorption curves of regenerated cellulose and nanocomposites films.

4.5. Thermal stability analysis

The thermal behaviour of the cellulose/HNT regenerated via EMIMCl was studied using the thermogravimetric analysis (TGA) results as depicted in Fig. 6. It can be observed that the HNT loading affected the thermal behaviour of the nanocomposites films. The TGA image revealed that as low as 1 wt% of HNT (C1), was able to significantly improve the RC nanocomposite films thermal behaviour. As the HNT loadings increase, the thermal behaviour was shifted towards higher temperature compared to neat cellulose. The film with 5 wt% HNT loading (C5) shows higher thermal stability compared to lower HNT loadings. This showed that the HNT inhibited the cellulose degradation (Liu, Jia, Liu, Jia, & Guo, 2010). The improvement of the thermal stability of the films was attributed to the strong interaction between cellulose and HNT. The thermal stability was enhanced due to the entrapment of the degradation products of the RC inside the lumen structure of the tubular rod of the HNT and good dispersion of the HNT in between the cellulose nanocomposites (Ismail et al., 2008).

The result also showed that the char residue of neat cellulose was fewer compared to the film with the HNT. Due to the formation of carbonaceous materials at elevated temperature, the char yield of the RC with HNT is high (Zhang et al., 2007). The HNT hindered the polymer form contacting with heat, therefore notably enhance the thermal degradation stability.

4.6. Water absorption analysis

Water absorption analysis was carried out in order to determine moisture absorption rate of the fabricated RC nanocomposites films incorporated with HNT. The result of the water absorption analysis was depicted in Fig. 7. It can be observed that the pure RC films, C has higher equilibrium water content compared to RC/HNT nanocomposites films. The water absorbency continues to reduce to minimal (7%) and (28%) with the HNT loadings of 1 wt% and 3 wt%, respectively. The water absorption decreased up to minimal (29%) when the HNT loading was gained up to 5 wt%. The existence of HNT in the RC nanocomposites films enhances the water resistance for the produced nanocomposites films.

The justification for the increment of water resistance with the increased of the HNT loadings was due to the existence of the watertight HNT particles which is a non-permeable materials, thus decline the rate of water permeable through the RC nanocomposites matrix. This was quite similar with previous report by Cyras, Manfredi, Ton-That, and Vázquez (2008) for MMT/starch nanocomposites.

5. Conclusions

This study presented an investigation on halloysite nanocomposites based on cellulose. The RC specimens were fabricated using EMIMCl, a 'green' solvent. The results showed the potential of HNT as nanofillers in polymer matrixes. It clearly displayed a good enhancement of both tensile strength and Young's modulus with HNT loading up to 5 wt %. As the HNT loadings increased to 5 wt%, the thermal behaviour and water resistance rate was also increased. The TEM and SEM images also depicted satisfactory dispersion of the HNT and good intertubular interaction between the HNT and the cellulose matrix. Remarkably, these findings were achieved using HNT at low loading (5 wt %) without any pretreatment, which suggests that there is a great potential for further improvement of the HNT/cellulose nanocomposites.

Acknowledgement

The authors would like to acknowledge the GUP research grant Vot 00H27 by Universiti Teknologi Malaysia.

References

Cao, Y., Wu, J., Zheng, J., Li, H., Zhang, Y., & He, J. (2009). Room temperature ionic liquids (RTILS): A new and versatile platform for cellulose processing and derivatization. *Chemical Engineering, 147*, 13–21.

Cyras, V. P., Manfredi, L. B., Ton-That, M. T., & Vázquez, A. (2008). Physical and mechanical properties of thermoplastic starch/montmorillonite nanocomposite films. *Carbohydrate Polymers, 73*, 55–63.

Delhom, C. D., White-Ghoorahoo, L. A., & Pang, S. S. (2010). Development and characterization of cellulose/clay nanocomposites. *Composites: Part B, 41*, 475–481.

Deng, S., Zhang, J., & Ye, L. (2009). Halloysite–epoxy nanocomposites with improved particle dispersion through ball mill homogenisation and chemical treatments. *Composites Science and Technology, 69*, 2497–2505.

Du, M., Guo, B., Lei, Y., & Jia, D. (2007). Thermal decomposition and oxidation ageing behaviour of polypropylene/halloysite nanotube nanocomposites. *Polymers and Polymer Composites, 15*, 321–328.

Feng, L., & Chen, Z. (2008). Research progress on dissolution and functional modification of cellulose in ionic liquids. *Molecular Liquids, 142*, 1–5.

Handge, U. A., Hedicke-Hochstotter, K., & Altstadt, V. (2010). Composites of polyamide 6 and silicate nanotubes of the mineral halloysite: Influence of molecular weight on thermal, mechanical and rheological properties. *Polymer*, *51*, 2690–2699.

Hedicke-Hochstotter, K., Lim, G. T., & Altstadt, V. (2009). Novel polyamide nanocomposites based on silicate nanotubes of mineral halloysite. *Composites Science and Technology*, *69*, 330–334.

Heinze, T., Schwikal, K., & Barthel, S. (2005). Ionic liquids as reaction medium in cellulose functionalization. *Macromolecule Bioscience*, *5*, 520–525.

Ismail, H., Pasbakhsh, P., Ahmad Fauzi, M. N., & Abu Bakar, A. (2008). Morphological, thermal and tensile properties of halloysite nanotubes filled ethylene propylene diene monomer (EPDM) nanocomposites. *Polymer Testing*, *27*, 841–850.

Levis, S. R., & Deasy, P. B. (2002). Characterisation of halloysite for use as a microtubular drug delivery system. *International Journal of Pharmaceutics*, *243*, 125.

Liu, M., Guo, B., Du, M., Chen, F., & Jia, D. (2009). Halloysite nanotubes as a novel (nucleating agent for isotactic polypropylene. *Polymer*, *50*, 3022–3030.

Liu, M., Jia, Z., Liu, F., Jia, D., & Guo, B. (2010). Tailoring the wettability of polypropylene surfaces with halloysite nanotubes. *Colloid and Interface Science*, *350*, 186–193.

Lopez Machando, M. A., Valentini, L., Biagiotti, J., & Kenny, J. M. (2005). Thermal and mechanical properties of single-walled carbon nanotubes–polypropylene composites prepared by melt processing. *Carbon*, *43*, 1499–1505.

Ma, H., Zhou, B., Li, H. S., Li, Y. Q., & Ou, S. Y. (2011). Green composites films composed of nanocrystalline cellulose and a cellulose matrix regenerated from functionalized ionic liquid solution. *Carbohydrate Polymers*, *84*, 383–389.

Mahmoudian, S., Wahit, M. U., Ismail, A. F., & Yussuf, A. A. (2012). Preparation of regenerated cellulose/montmorillonite nanocomposite films via ionic liquids. *Carbohydrate Polymers*, *88*, 1251–1257.

Ning, N. Y., Yin, Q. J., Luo, F., Zhang, Q., Du, R., & Fu, Q. (2007). Crystallization behavior and mechanical properties of polypropylene/halloysite composites. *Polymer*, *48*, 7374–7384.

Nishino, T., Matsuda, I., & Hirao, K. (2004). All-cellulose composite. *Macromolecules*, *37*, 7683–7687.

Prashantha, K., Lacrampe, M. F., & Krawczak, P. (2010). Processing and characterization of halloysite nanotubes filled polypropylene nanocomposites based on a masterbatch route: Effect of halloysites treatment on structural and mechanical properties. *eXPRESS Polymer Letter*, *5*, 295–307.

Rahatekar, S. S., Rasheed, A., Jain, R., Zammarano, M., Koziol, K. K., & Windle, A. H. (2009). Solution spinning of cellulose carbon nanotubes composites using room temperature ionic liquids. *Polymers*, *50*, 4577–4583.

Suresh, K. M., Yun, S., & Kim, J. (2011). Flexible humidity and temperature sensor based on cellulose–polypyrrole nanocomposites. *Sensor and Actuators A: Physical*, *165*, 194–199.

Takagi, H., & Asano, A. (2008). Effects of processing condition on flexural properties of cellulose nanofiber reinforced 'green' composites. *Composites Part A: Applied Science and Manufacturing*, *39*, 685–689.

Tang, Y., Deng, S., Ye, L., Yang, C., Yuan, Q., Zhang, J., & Zhao, C. (2011). Effects of unfolded and intercalated halloysites on mechanical properties of halloysite–epoxy nanocomposites. *Composites: Part A*, *42*, 345–354.

Tang, X. Z., Kumar, P., Alari, S., & Sandeep, K. P. (2012). Recent advance in biopolymers and biopolymer-based nanocomposites for food packaging materials. *Food and Science Nutrition*, *52*, 426–442.

Vadukumpully, S., Paul, J., Mahanta, N., & Valiyaveettil, S. (2011). Flexible conductive graphene/poly(vinyl chloride) composite thin films with high mechanical strength and thermal stability. *Carbon*, *49*, 198–205.

Vergaro, V., Abdullayev, E., Lvov, Y. M., Zeitoun, A., Cingolani, R., Rinaldi, R., & Leporatti, St. (2010). Cytocompatibility and uptake of halloysite clay nanotubes. *Biomacromolecules*, *11*, 820–826.

Vitz, J., Edmenger, E., Haensch, C., & Schubert, U. S. (2009). Extended dissolution studies of cellulose in imidazolium based ionic liquids. *Green chemistry*, *11*, 417–424.

Wu, R. L., Wanga, X. L., Li, F., Li, H. Z., & Wanga, Y. Z. (2009). Green composite films prepared from cellulose, starch and lignin in room-temperature ionic liquid. *Bioresource Technology*, *100*, 2569–2574.

Ye, Y., Chen, H., Wu, J., & Ye, L. (2007). High impact strength epoxy nanocomposites with natural nanotubes. *Polymer*, *48*, 6426.

Zhang, H., Wang, Z., Zhang, Z., Wu, J., Zhang, J., & He, J. (2007). Regenerated cellulose multiwalled-carbon-nanotube composites fibers with enhanced mechanical properties prepared with the ionic liquid 1-ally-3-methylinidazolium chloride. *Advanced Material*, *19*, 698–704.

Zhao, D., Li, H., Zhang, J., Fu, L., Lim, M., Fu, J., & Ren, P. (2012). Dissolution of cellulose in phosphate-based ionic liquid. *Carbohydrate Polymers*, *87*, 1490–1494.